Science Bulletin 64 (2019) 1764–1772

Contents lists available at ScienceDirect

Science Bulletin

journal homepage: www.elsevier.com/locate/scib

Science Bulletin
www.scibull.com

Article

Glycerol aerobic oxidation to glyceric acid over Pt/hydrotalcite catalysts at room temperature

Junbo Zhang [a], Xiaolin Li [a], Ming Xu [b], Yusen Yang [a], Yinwen Li [a], Ning Liu [a], Xiaoyu Meng [a], Lifang Chen [a], Shuxian Shi [a,*], Min Wei [a,*]

[a] State Key Laboratory of Chemical Resource Engineering, Beijing Advanced Innovation Center for Soft Matter Science and Engineering, Beijing University of Chemical Technology, Beijing 100029, China
[b] College of Chemistry and Molecular Engineering and College of Engineering, BIC-ESAT, Peking University, Beijing 100871, China

ARTICLE INFO

Article history:
Received 16 July 2019
Received in revised form 31 August 2019
Accepted 24 September 2019
Available online 4 October 2019

Keywords:
Rehydrated hydrotalcites
Interfacial structure
Support basicity
Active sites
Rate-determining step

ABSTRACT

Glycerol (GLY) aerobic oxidation in an aqueous solution is one of the most prospective pathways in biomass transformation, where the supported catalysts based on noble metals (mainly Au, Pd, Pt) are most commonly employed. Herein, Pt nanoparticles supported on rehydrated Mg_xAl_1-hydrotalcite (denoted as re-Mg_xAl_1-LDH-Pt) were prepared via impregnation-reduction method followed by an *in situ* rehydration process, which showed high activity and selectivity towards GLY oxidation to produce glyceric acid (GLYA) at room temperature. The metal-support interfacial structure and catalyst basicity were modulated by changing the Mg/Al molar ratio of the hydrotalcite precursor, and the optimal performance was achieved on re-Mg_6Al_1-LDH-Pt with a GLY conversion of 87.6% and a GLYA yield of 58.6%, which exceeded the traditional activated carbon and oxide supports. A combinative study on structural characterizations (XANES, CO-FTIR spectra, and benzoic acid titration) proves that a higher Mg/Al molar ratio promotes the formation of positively charged $Pt^{\delta+}$ species at metal-support interface, which accelerates bond cleavage of α-C–H and improves catalytic activity. Moreover, a higher Mg/Al molar ratio provides a stronger basicity of support that contributes to the oxidation of terminal-hydroxyl and thus enhances the selectivity of GLYA. This catalyst with tunable metal-support interaction shows prospective applications toward transformation of biomass-based polyols.

1. Introduction

Biodiesel, a favorable alternative fuel acquired sustainably from animal or vegetable fats, is becoming increasingly attractive worldwide due to the depletion of fossil fuels [1,2]. As the unavoidable by-product of biodiesel manufacture, glycerol is growing excessively with the increasing production volume of biodiesel [3–5]. Therefore, glycerol transformations including oxidation, hydrogenlysis, esterification, and reforming have become increasingly significant in terms of economy and environmental protection [6–10], creating an array of value-added products as well [11,12]. Among these transformation approaches, glycerol selective oxidation in aqueous phase over heterogeneous nanoparticles (NPs) is quite promising due to its diverse products of functionalized molecule including glyceraldehyde (GLYD), glyceric acid (GLYA), dihydroxyacetone (DHA), tartronic acid (TTA), glycolic acid (GLCOA), oxalic acid (OXA), and so on [13,14]. Although extensive efforts have been made toward catalytic oxidation of glycerol, how to control selectivity of specific product and to reveal structure-property correlation of catalysts still remain lacking and challenging [15–17].

In virtue of their high oxidation ability, Pt NPs loaded on various supports have attracted considerable attention in the oxidation of biomass-based polyols [18,19]. The direct catalytic oxidation of glycerol to GLYA has been studied for decades, and Pt-based catalysts have shown satisfactory behavior for GLYA generation [20,21]. In attaining a single product selectively with a high conversion meanwhile, support effect should be taken as priority, since metal-support interaction plays a vital role in heterogeneous catalysis [22,23]. For instance, Yu and co-workers [24] reported an efficient N-doped carbon supported Pt catalyst for aerobic oxidation of glycerol, where nitrogen dopant obviously improved the dispersion of Pt NPs with enhanced metal-support interaction and promoted catalytic performance. Hou and co-workers [25] developed Pt NPs encapsulated inside carbon film and found that coating effect from multi-walled carbon nanotubes (MCNTs)

* Corresponding authors.
E-mail addresses: shisx@mail.buct.edu.cn (S. Shi), weimin@mail.buct.edu.cn (M. Wei).

https://doi.org/10.1016/j.scib.2019.10.003
2095-9273/

impeded the aggregation of Pt NPs and thus induced largely enhanced stability. In spite of these studies, few succeed to elucidate the significance of metal-support interaction in boosting the catalytic performance and understanding on structure-activity relationship remains ambiguous.

In this work, Pt NPs supported on a series of layered double hydroxides (LDHs) were prepared through a facile wet impregnation method followed by an *in situ* rehydration procedure. The Mg/Al molar ratio of LDH support was modified, through which the interfacial structure and support basicity were optimized to serve glycerol oxidation under a base-free condition at room temperature. A combination study involving X-ray absorption fine structure (XAFS) spectroscopy, *in situ* Fourier transform infrared spectroscopy, H_2-TPR and catalytic evaluations confirms that the electrons-deficient $Pt^{\delta+}$ species contribute to the significantly enhanced catalytic activity via promoting α-C–H bond cleavage. The results show that a moderate basicity of catalyst is favorable to the selectivity of GLYA. Taking into account the trade-off between conversion and selectivity, re-Mg_6Al_1-LDH-Pt was employed as the optimal catalyst, giving a GLYA yield of 58.6% that is at a high level among previous studies performed at room temperature.

2. Experimental

2.1. Materials

$H_2PtCl_6{\cdot}6H_2O$ (38 wt%–40 wt% Pt) were purchased from J&K. $Mg(NO_3)_2{\cdot}6H_2O$ (99.99 wt% purity), $Al(NO_3)_3{\cdot}9H_2O$ (99.9 wt% purity), NaOH (99 wt% purity) and Na_2CO_3 (99.5 wt% purity) were all purchased from Aladdin.

2.2. Catalysts preparation

2.2.1. Preparation of Mg_xAl_1-LDH

Mg_xAl_1-LDH (x = 2, 4, 6, 8) precursors were synthesized by a co-precipitation method [26]. Typically, $Mg(NO_3)_2$ and $Al(NO_3)_3$ were dissolved in water (100 mL) to form a mixed salt solution (M = $[Mg^{2+}] + [Al^{3+}]$ = 0.4 mol L^{-1}); NaOH and Na_2CO_3 were also dissolved in water (100 mL) to form an alkaline solution ($[OH^-]$ = 1.6 mol L^{-1}, $[CO_3^{2-}] = 2[Al^{3+}]$). These two solutions were added dropwise simultaneously (1.0 mL min^{-1}) into a flask with constant stirring. The pH value of slurry was kept at 10.0 ± 0.2 at room temperature. Afterwards, the slurry was aged at 90 °C for 24 h, centrifuged, washed with water and ethanol, and finally dried at 60 °C overnight. As a control sample, $Mg(OH)_2$ was prepared by a precipitation method similar to Mg_xAl_1-LDH. $Mg(NO_3)_2$ solution (0.4 mol L^{-1}, 100 mL) and NaOH solution (0.64 mol L^{-1}, 100 mL) were added dropwise and simultaneously (1.0 mL min^{-1}) into a flask with constant stirring, with the pH value keeping at 10.0 ± 0.2. Afterwards, the slurry was aged at 90 °C for 24 h, centrifuged, washed with water and ethanol, and finally dried at 60 °C overnight.

2.2.2. Preparation of Mg_xAl_1-LDH-Pt

Mg_xAl_1-LDH supported Pt samples were prepared with wet impregnation. In a typical procedure, 0.5 g of Mg_xAl_1-LDH was dispersed in 40 mL of water with ultrasonic treatment for 20 min to obtain a uniform suspension. Subsequently, 0.5 mL of $H_2PtCl_6{\cdot}6H_2O$ aqueous solution (26.55 mg mL^{-1}) was dropped into the suspension, followed by stirring at room temperature overnight. Finally, the sample was dried at 60 °C to obtain catalyst precursor Mg_xAl_1-LDH-Pt.

2.2.3. Preparation of re-Mg_xAl_1-LDH-Pt

Mg_xAl_1-LDH-Pt sample was reduced in a H_2/N_2 (10 vol%) flow at 350 °C for 3 h, with a heating rate of 5 °C min^{-1}. Mg_xAl_1-LDH-Pt catalyst precursor transformed into Mg_xAl_1-MMO supported Pt catalyst (named Mg_xAl_1-MMO-Pt). After reduction and cooling, Mg_xAl_1-MMO-Pt sample was sealed within GLY aqueous solution to acquire re-Mg_xAl_1-LDH-Pt via rehydration process [27].

2.3. Catalysts evaluation

Glycerol oxidation reaction was carried out in a batch-type reactor (cylindrical glass tube) connected with a balloon filled with oxygen as gas replenishment. As the reactor temperature was stabilized at 30 °C, O_2 was introduced into the reactor to initiate the oxidation reaction. The kinetic isotope effect was studied on the oxidation of ethanol over re-Mg_6Al_1-LDH-Pt using unlabeled C_2H_5OH and deuterium-labeled C_2H_5OD for the reaction.

Reaction conditions were as follows: 30 °C reaction temperature (defined as room temperature in this work), ambient pressure, 20 mL of GLY aqueous solution (0.1 mol L^{-1}) and 39 mg of catalyst (GLY/Pt = 1000). After reaction, the solution was filtered using a hydrophilic filter. The reactant conversion and product selectivity were analyzed by an Agilent 1200 series high-performance liquid chromatograph (HPLC) fitted with a refractive index detector (RID) and a ultraviolet detector (UVD) with an Aminex HPX-87H column (7.8 mm × 300 mm, Bio-Rad). The mobile phase was H_2SO_4 aqueous solution (0.01 mol L^{-1}) and the flow rate was 0.6 mL min^{-1} at a column temperature of 50 °C. Specially, glyceraldehyde was distinguished from glyceric acid using HCOOH aqueous solution (0.01 mol L^{-1}) as mobile phase. The products identified by chemical standards were quantified with external standard method. The conversion and the selectivity were calculated as following:

$$\text{Conversion}\ (\%) = \frac{\text{mol of glycerol converted}}{\text{mol of glycerol before reaction}} \times 100, \quad (1)$$

$$\text{Selectivity}\ (\%) = \frac{(\text{mol of product}) \times (\text{carbon atom number of the product})}{(\text{mol of glycerol reacted}) \times 3} \times 100. \quad (2)$$

Turnover frequency (TOF) was calculated as the amount of glycerol reacted per hour per surface Pt site which was attained from the Pt dispersion (dispersion = 1.13/size) [28,29].

2.4. Catalysts characterization

The X-ray powder diffraction (XRD) measurements were implemented on a Rigaku XRD-6000 diffractometer, using Cu Kα radiation (λ = 0.15418 nm) at 40 kV, 40 mA, with a scanning rate of 10° min^{-1} and a 2θ angle from 3° to 70°. *Quasi in situ* X-ray absorption fine structure (XAFS) in Pt L_{III}-edge was measured in fluorescence mode at ambient temperature at beam line 1W2B of Beijing Synchrotron Radiation Facility (BSRF), Institute of High Energy Physics (IHEP), Chinese Academy of Sciences (CAS). Pt foil and PtO_2 were used as reference samples. In prior to the experiment, 60 mg of re-Mg_xAl_1-LDH-Pt was pressed into a disk with a diameter of 13 mm. After reduction at 200 °C for 1 h, it was transferred into glove box and sealed in Ar atmosphere. The obtained XANES spectra were analyzed using the Athena program of IFFEFIT 1.2.11 package.

The morphology of the samples was investigated using a Zeiss Supra 55 scanning electron microscope (SEM) operating with an accelerating voltage of 20 kV. Transmission electron microscopy (TEM) and high resolution TEM (HRTEM) experiments were performed using a JEOL JEM-2100 transmission electron microscope at a voltage of 200 kV. Multipoint Brunauer-Emmett-Teller (BET) method was adopted to evaluate the total specific surface area using low-temperature N_2 adsorption-desorption. The chemical

composition of the samples was measured with inductively coupled plasma-atomic emission spectrometer (ICP-AES). Hydrogen temperature-programmed reduction (H2-TPR) was performed on a Micrometric ChemiSorb 2720 chemisorption system equipped with a thermal conductivity detector (TCD). Before measurement, 0.1 g of the Mg_xAl_1-LDH-Pt sample was sealed in a Utype quartz tube, followed by pretreatment in Ar atmosphere at 200 °C for 2 h. Then, the sample was reduced in a flow of H_2/Ar (10 vol%, 40 mL min^{-1}) from 50 to 900 °C at a heating rate of 10 °C min^{-1}.

In situ FTIR transmission spectrum of CO adsorption was carried out at 30 °C to investigate the chemical state of Pt NPs. It was performed on a Bruker TENSOR II spectrometer, ranging from 4000 to 850 cm^{-1} with a resolution of 4 cm^{-1}. Before measurement, 25 mg of re-Mg_xAl_1-LDH-Pt was reduced at 200 °C in a H_2/N_2 (10 vol%) flow for 1 h in the sample cell and then evacuated with He at 30 °C for 20 min to obtain a reference baseline signal. Afterwards, CO/He (5 vol%) was introduced into the cell for another 60 min. Then He was introduced again to eliminate the physically adsorbed CO and infrared signal vs. the reference signal was recorded.

Titration was performed to determine the basicity of the catalyst. In the measurement, 0.01 g bromothymol blue was dissolved in 100 mL of toluene to obtain an acid-base indicator. Then, 0.2 g of re-Mg_xAl_1-LDH was suspended in 2 mL of indicator solution and the suspension was titrated with a solution of benzoic acid dissolved in toluene (0.01 mol L^{-1}).

3. Results and discussion

3.1. Structural and morphological characterizations

Mg_xAl_1-LDH precursors with Mg/Al molar ratio ranging from 2 to 8 were synthesized by co-precipitation method. The XRD patterns (Fig. 1a) display the (0 0 3), (0 0 6), (0 0 9), (1 1 0) diffraction peak at ~11.6°, 23.6°, 35.5° and 61.2°, respectively, corresponding to a typical LDHs structure [26]. From Mg_2Al_1-LDH to Mg_8Al_1-LDH, a shift of reflections to a lower 2θ indicates a gradually increased basal spacing, resulting from a decreased charge density of LDHs host matrix and weaker host-guest electrostatic interactions. After impregnation with Pt, no obvious change is found in the XRD patterns of Mg_xAl_1-LDH-Pt samples (Fig. S1a online). The following reduction procedure results in the formation of Mg_xAl_1-MMO-Pt, whose XRD patterns show reflections assigned to MgO phase (Fig. 1b). After a subsequent *in situ* rehydration treatment, re-Mg_xAl_1-LDH-Pt samples were obtained with an LDH structure (Fig. 1c) which are identical with Mg_xAl_1-LDH. No diffraction peak attributed to Pt species is observed in Mg_xAl_1-LDH-Pt, Mg_xAl_1-MMO-Pt and re-Mg_xAl_1-LDH-Pt, due to a low loading of Pt and/or a high metal dispersion.

SEM images of Mg_xAl_1-LDH-Pt samples are shown in Fig. S2a (online), and the plate-like morphology is observed with particle size of 200–500 nm. With the increase of Mg/Al ratio from 2 to 8, the SEM images show no significant difference in morphology. The rehydrated samples re-Mg_xAl_1-LD-Pt inherit the initial flake morphology (Fig. S2b online), which underwent second crystallization to form twisted LDHs layers. TEM and HRTEM were used to investigate sample structure and particle size (Fig. 2). Notably, as the Mg/Al ratio rises from 2 to 8, the mean size of Pt NPs increases from 1.7 to 2.9 nm. In addition, HRTEM images exhibit an apparent lattice fringe distance of ~0.221 nm, corresponding to the (1 1 1) plane of metallic Pt for samples except re-Mg_2Al_1-LDH-Pt due to its rather small particle size (less than 2 nm).

Re-Mg_xAl_1-LDH-Pt samples were also studied with low-temperature N_2 adsorption-desorption to investigate the specific surface area and the pore-size distribution (Table S1 and Fig. S3 online). All these samples exhibit IV type isotherms with H3 shaped hysteresis loops, which correspond to the typical mesoporous materials. As listed in Table S1 (online), with the increment of Mg/Al ratio, the specific surface area increases from 89.1 to 133.4 m^2 g^{-1} and then decreases dramatically to 25.1 m^2 g^{-1}. The specific surface area value of re-Mg_4Al_1-LDH-Pt is the largest. The actual Mg/Al ratio and Pt loading are determined by inductively coupled plasma atomic emission spectrometer (ICP-AES), which accord with the theoretical values. In addition, re-Mg_xAl_1-LDH-Pt samples were titrated with benzoic acid dissolved in toluene and the amount of basic sites was labeled using the amount of benzoic acid used per mass of sample [30–32]. As listed in Table 1, the concentration of surface basic sites increases with the enhancement of Mg^{2+} content, from 0.07 mmol g^{-1} (re-Mg2Al1-LDH-Pt) to 0.27 mmol g^{-1} (re-Mg_8Al_1-LDH-Pt).

3.2. The electronic structure of re-Mg_xAl_1-LDH-Pt

In order to understand the structural properties of catalysts, XANES spectroscopy (Fig. 3a) and *in situ* FTIR spectrum (Fig. 3b) were performed. In general, the intensity of white line in XANES spectra represents the d-band electron vacancy, by which the oxidation state can be determined with Pt foil and PtO_2 as reference [33]. As revealed from XANES spectra at Pt L-edge in Fig. 3a, all the samples with different Mg/Al ratios demonstrate valence state between Pt foil and PtO_2, although those white lines are more close to Pt foil. This indicates that Pt nanoparticle is comprised of a vast majority of metallic platinum (denoted as Pt^0) accompanied with a minority of oxidized platinum (denoted as $Pt^{\delta+}$). From re-Mg_2Al_1-

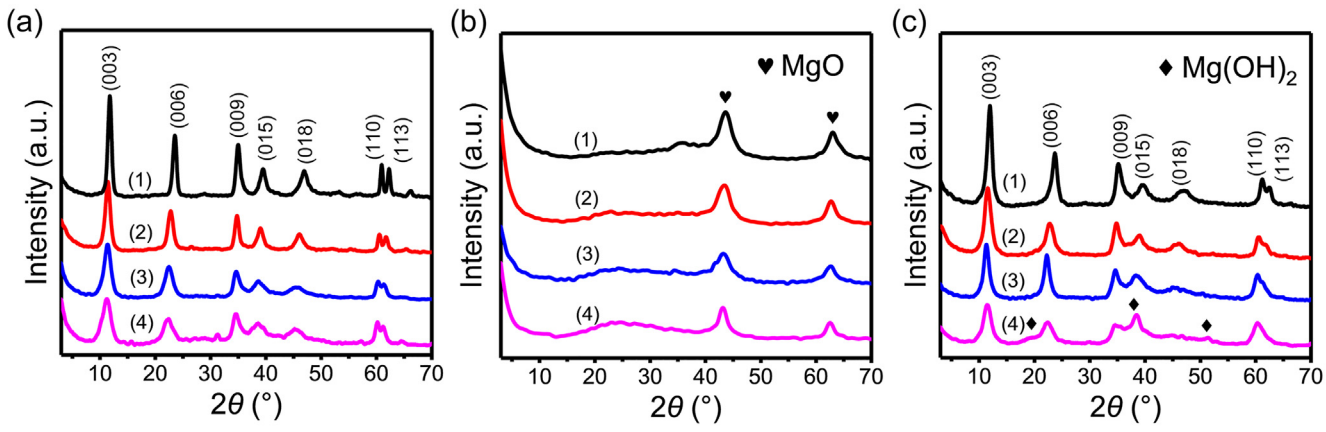

Fig. 1. (Color online) XRD patterns of (a) Mg_xAl_1-LDH, (b) Mg_xAl_1-MMO-Pt and (c) re-Mg_xAl_1-LDH-Pt. (1) Mg/Al = 2; (2) Mg/Al = 4; (3) Mg/Al = 6; (4) Mg/Al = 8.

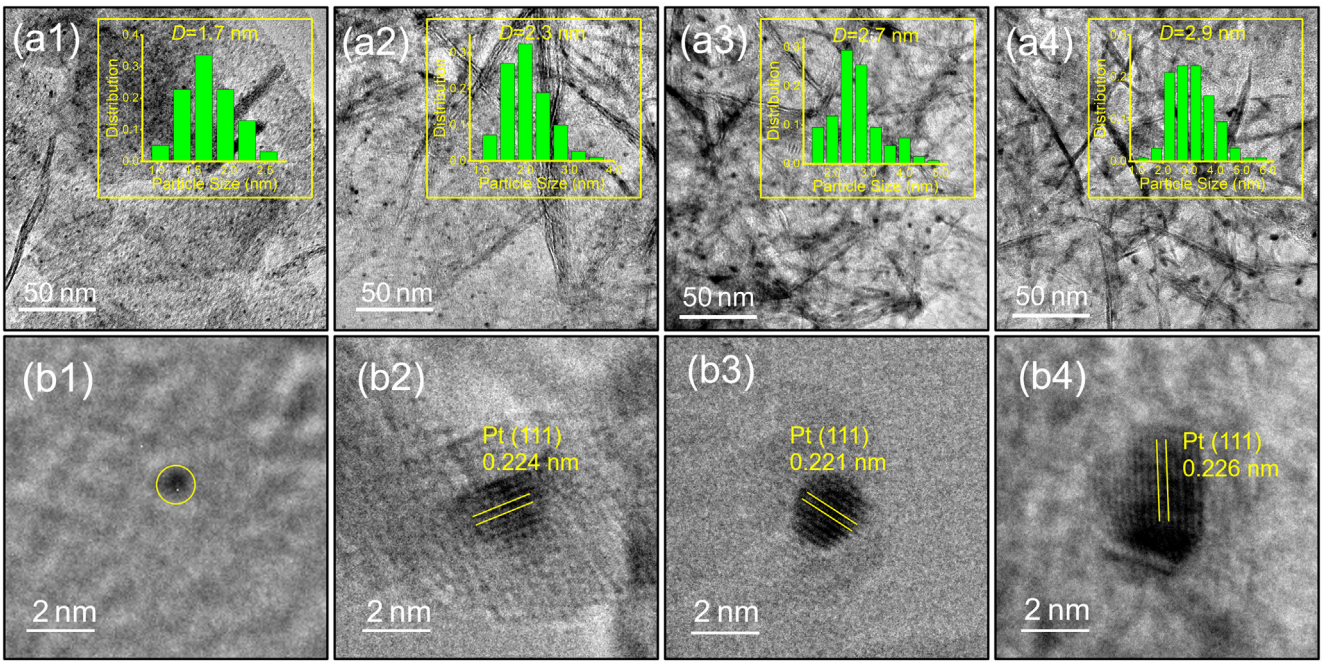

Fig. 2. (Color online) TEM (a1–a4) and HRTEM (b1–b4) images of re-Mg_xAl_1-LDH-Pt catalysts. (a1, b1): Mg/Al = 2; (a2, b2): Mg/Al = 4; (a3, b3): Mg/Al = 6; (a4, b4): Mg/Al = 8. Inset: the histogram of size distribution of Pt nanoparticles.

Table 1
Basicity, composition and Pt nanoparticles characterizations.

Samples	Basic sites[a] (mmol g^{-1})	Mg/Al[b] (mol:mol)	Pt loading[c] (wt%)	Mean Pt size[d] (nm)	$Pt^{\delta+}/(Pt^0 + Pt^{\delta+})$[e] (mol:mol)
re-Mg_2Al_1-LDH-Pt	0.07	1.9	0.90	1.7	0.18
re-Mg_4Al_1-LDH-Pt	0.18	3.7	1.14	2.3	0.25
re-Mg_6Al_1-LDH-Pt	0.23	5.3	0.91	2.7	0.32
re-Mg_8Al_1-LDH-Pt	0.27	6.9	0.87	2.9	0.56

[a] Determined by titration of benzoic acid.
[b] and [c] determined by ICP-AES.
[d] Determined by TEM for Pt particles supported on corresponding support.
[e] Determined by the deconvolution of *in situ* FTIR in Fig. 3b.

LDH-Pt to re-Mg_8Al_1-LDH-Pt, the intensity of white-edge becomes more pronounced, indicating that more $Pt^{\delta+}$ species generate with the increase of Mg content. Nevertheless, it is rather difficult to determine the exact charge of Pt species, owing to the lacking of standard sample. We will further resolve this issue in our future work.

Unfortunately, it is hard to obtain distinct coordination of Pt–O bond on the surface since X-ray absorption spectroscopy is insensitive to surface structure. For this reason, *in situ* FTIR spectroscopy was carried out to further explore the surface chemical environment. After the introduction of CO into the re-Mg_xAl_1-LDH-Pt system as a probe, the doublet peaks at 2172 and 2129 cm^{-1} appear immediately, which are attributed to vibrations of gaseous CO (Fig. S4 online). After purging with He, the bands of gaseous CO for all these four samples become weaker and disappear ultimately after 6 min. Two dominant bands (2106–1997 and 1856–1772 cm^{-1}) are observed stably, which can be attributed to the linearly bonded CO on Pt atom and the bridge-bonded CO on two adjacent Pt atoms, respectively [34]. From re-Mg_2Al_1-LDH-Pt to re-Mg_8Al_1-LDH-Pt, the strength of linear adsorption weakens gradually whereas that of CO bridge adsorption enhances accordingly, in accordance with the increased particle size of Pt observed by TEM. Unexpectedly, the linear adsorption band (2106–1997 cm^{-1}) splits into two bands centered at 2069 and 2035 cm^{-1}, respectively. As reported previously [35], the variation in electron density of transition metal imposes influences on the back-donation of d-electrons to the $2\pi^*$ antibonding orbital of CO, which would result in the change of C–O bond strength and the shift of stretching frequency. In this work, the splitting of CO linear adsorption band can be explained as the coexistence of electron-rich Pt^0 and electron-deficient $Pt^{\delta+}$ species [36,37]. The IR band is therefore deconvoluted into two peaks via a Gaussian peak fitting method [38], so as to estimate the relative content of $Pt^{\delta+}$ on the sample surface (Fig. 3b). With the increment of Mg/Al ratio in LDH supports, $Pt^{\delta+}/(Pt^{\delta+} + Pt^0)$ ratio rises gradually, which agrees well with the results of XANES.

H_2-TPR measurements were carried out on Mg_xAl_1-LDH-Pt samples to study their reducibility (Fig. S1b online), in which two peaks at ~280 and ~440 °C were observed for all these four samples. The peak at low temperature can be assigned to the reduction of Pt species at oxidation state, while the one at high temperature is the disruptive TCD signal of CO_2 originated from thermal decomposition of LDHs in temperature programmed process. Interestingly, the reduction temperature for oxidized Pt species rises gradually from 262 to 305 °C as Mg/Al ratio of Mg_xAl_1-LDH-Pt increases from 2 to 8, suggesting a progressively enhanced metal-support interaction

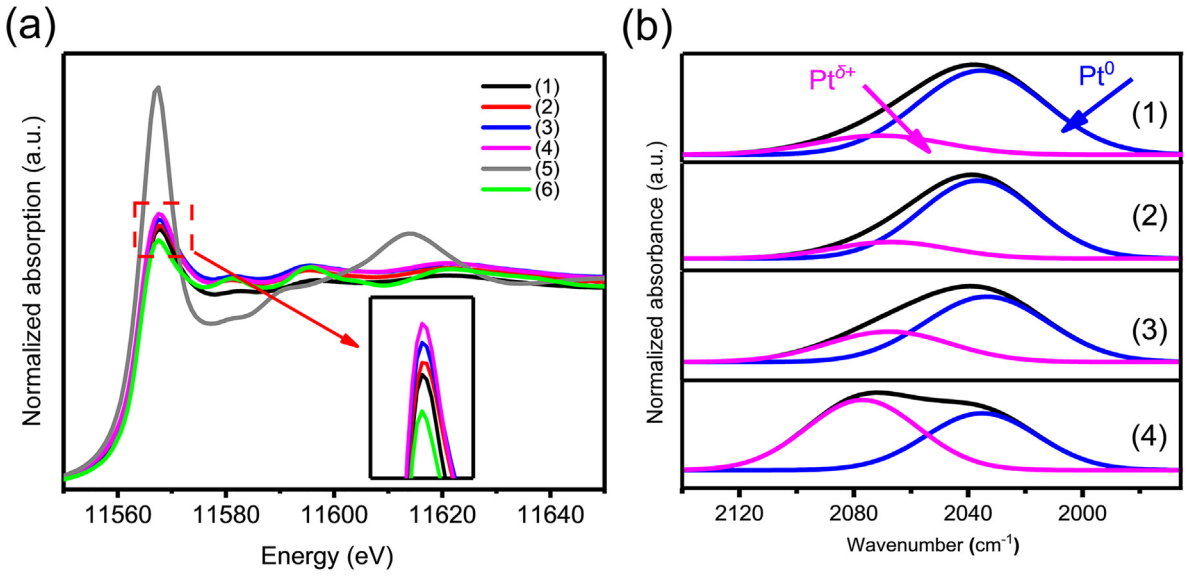

Fig. 3. (Color online) Structural information of re-Mg_xAl_1-LDH-Pt nanostructures. (a) Normalized *quasi in situ* XANES spectra at Pt L-edge for re-Mg_xAl_1-LDH-Pt samples. Inset: the enlarged view of selected white line from (a). (b) *In situ* FTIR transmission spectra on re-Mg_xAl_1-LDH-Pt samples after saturated adsorption of CO followed by evacuation with He at 30 °C for 20 min. (1) Mg/Al = 2; (2) Mg/Al = 4; (3) Mg/Al = 6; (4) Mg/Al = 8; (5) PtO_2; (6) Pt foil.

Table 2
Effect of Mg/Al ratio on the activity of GLY oxidation.[a]

Catalysts	TOF[b] (h^{-1})	Conversion (%)	Product selectivity (%)				C-balance[d] (%)
			GLYA	DHA	TTA	C_2[c]	
re-Mg_2Al_1-LDH-Pt	93.5	16.6	64.8	20.5	0.4	2.0	87.8
re-Mg_4Al_1-LDH-Pt	166.7	29.0	74.3	19.2	1.1	2.5	97.1
re-Mg_6Al_1-LDH-Pt	241.1	34.9	77.0	16.8	2.4	1.9	98.2
re-Mg_8Al_1-LDH-Pt	341.8	45.8	73.0	15.9	2.5	4.6	95.9
re-$Mg(OH)_2$-Pt	281.7	33.2	49.7	14.4	5.5	10.4	79.9

[a] Reaction conditions: 20 mL glycerol aqueous solution (0.1 mol L^{-1}), GLY/Pt = 1000, 30 °C, ambient pressure, 10 h.
[b] TOF is based on surface Pt atoms when the conversion of glycerol was 20%.
[c] C_2 product selectivity is the sum selectivity of glycolic acid and oxalic acid.
[d] C-balance represents the total selectivity of the liquid products.

[39,40]. This coincides with the results of XAFS and CO-FTIR where more $Pt^{\delta+}$ species are formed with the increase of Mg/Al ratio.

3.3. Catalytic performance of re-Mg_xAl_1-LDH-Pt

The catalytic oxidation reaction of glycerol was performed in a batch glass tube reactor equipped with a balloon as oxygen replenishment at room temperature. GLYD and DHA are the two initial products, originating from the oxidation of terminal-hydroxyl and central-hydroxyl, respectively. Specially, GLYD is apt to convert immediately to GLYA once generated [41], which accounts for its absence in the course of reaction. As shown in Table 2, GLY conversion increases from 16.6% to 45.8% and TOF value increases from 93.5 to 341.8, as the Mg/Al ratio rises from 2 to 8. The highest conversion (45.8%) is attained by re-Mg_8Al_1-LDH-Pt which also exhibits the highest TOF value (341.8 h^{-1}). From the time course of re-Mg_xAl_1-LDH-Pt conversion (Fig. S5 online), GLY conversion of re-Mg_8Al_1-LDH-Pt is dominant at any time point. In contrast, re-$Mg(OH)_2$-Pt sample shows a lower activity compared with re-Mg_xAl_1-LDH-Pt samples, which could be ascribed to its enlarged particle size and decreased metal dispersion (Fig. S6 online). In addition, the carbon balance (C-balance) of >92% for the liquid products was detected over re-Mg_xAl_1-LDH-Pt catalysts except for re-Mg_2Al_1-LDH-Pt, probably due to some abnormal products that cannot be identified under the current analysis condition.

GLYA and DHA are the two main products obtained in this reaction, and the other products from over-oxidation (TTA) and C–C bond fracture (C_2 products) can also be found (Table 2). For example, the contents of TTA and C_2-products (glycolic acid and oxalic acid) rise with the increase of Mg/Al ratio but both of them show the lower selectivity (2.4% and 1.9%) compared with previous reports (>5% and >4%) [42,43]. This is likely attributed to the lower reaction temperature in this work (room temperature), which leads to less extent of side reaction. The selectivity of GLYA increases from 64.8% (re-Mg_2Al_1-LDH-Pt) to 77.0% (re-Mg_6Al_1-LDH-Pt), and then declines to 73.0% (re-Mg_8Al_1-LDH-Pt), whilst the DHA selectivity decreases monotonously along with the increment of Mg/Al ratio (from 20.5% to 14.4%). As for re-$Mg(OH)_2$-Pt, although the conversion of GLY is higher than both re-Mg_2Al_1-LDH-Pt and re-Mg_4Al_1-LDH-Pt, the selectivity of GLYA is quite low and the selectivity of both TTA and by-products (TTA and C_2-products) is higher than re-Mg_xAl_1-LDH-Pt samples. Taking into account both GLYA selectivity and GLY conversion, re-Mg_6Al_1-LDH-Pt is thus chosen as the target catalyst.

Afterwards, we explored the effect of catalyst amount on the catalytic performance, where the molar ratio of reactant to Pt changed. From the complex reaction pathways in glycerol oxidation, parallel reaction is accompanied with a series of consecutive

reactions. Particularly, GLYA is determined not only by the preference degree between α-OH and β-OH but also by the degree of over-oxidation related to the amount of catalyst used. From the time course curves of conversion in Fig. 4a, it is found that the conversion increases along with the catalyst weight at any time, which corresponds to the batch reaction in theory. For re-Mg_6Al_1-LDH-Pt catalyst with a GLY/Pt ratio of 1000, the conversion keeps increasing before it reaches equilibrium maximum 64% at 22 h. The maximum conversions for GLY/Pt = 500 and GLY/Pt = 250 attain to 91% at 18 h and to 94% at 14 h, respectively. However, the trend of GLYA yield does not agree with the trend as conversion. Fig. 4b elucidates that all the experiments with different catalyst weight show volcanic curves of yield vs. time, whose decline disclose a severe over-oxidation. When the GLY/Pt ratio is 1000 (Fig. 4b), the GLYA yield starts to decline at 20 h, indicating that the speed of over-oxidation exceeds that of GLYA formation at that time. The maximum yield is 49.8% for GLY/Pt = 1000 as a result of the lower conversion in the whole process. In the case of GLY/Pt = 250, the decline of yield occurs at 8 h (maximum: 46%) in spite of the highest conversion. Among the experiments with different catalyst weight, an optimum GLYA yield of 59% is achieved over re-Mg_6Al_1-LDH-Pt with GLY/Pt = 500, which is at a high level compared with the previous reports of glycerol oxidation (normally below 55%). This validate that an opportune catalyst dosage is demanding for a batch reaction. The distribution of products is illustrated in Fig. 4c, where GLYA selectivity declines and TTA selectivity rises with the increment of catalyst weight. This verifies an enhanced extent of over-oxidation with a high level of catalyst used. However, DHA is nearly immune to catalyst weight, with only a slight decrease in selectivity as GLY/Pt ratio attains 250. C_2-products including GLCOA and OXA are always monitored with a lower sum selectivity compared with previous reports. One of the primary reasons lies in the truth that a low temperature (e.g., room temperature) inhibits the occurrence of side reactions. The recycling measurements were carried out to test the reusability of Mg_6Al_1-LDH-Pt (Fig. 4d). To remove the oxygenates absorbed on catalyst surface, we performed a regeneration process after each run: the used catalyst was centrifuged, washed and dried, followed by reduction at 350 °C for 3 h and the final *in situ* rehydration in GLY aqueous solution for 1 h [44]. GLY conversion declines from 87.6% to 76.9% (a decrease of 10.7%) and GLYA yield drops from 58.6% to 46.1% (a decrease of 12.5%) after four runs.

4. Discussions on structure-property correlation

For alcohol aerobic oxidation reactions, the identification of rate-determining step (the breakage of O–H bond vs. α-C–H bond) is under controversy for a long time. To understand this issue, the study on kinetic isotope effect (KIE) was carried out on the oxidation of ethanol as a probe molecule over re-Mg_6Al_1-LDH-Pt, by comparing the activity of C_2H_5OD with non-labeled C_2H_5OH. As shown in Fig. 5, a linear relationship is obtained between $\ln(C_{A0}/C_A)$ (C_A represents the concentration of ethanol and C_{A0} is the initial concentration) and reaction time, demonstrating the first order reaction with respect to ethanol. The rate constants measured with C_2H_5OH and C_2H_5OD are $k_H = 0.0812\ h^{-1}$ and $k_D = 0.0621\ h^{-1}$, respectively, giving a KIE of $k_H/k_D = 1.31$. This indicates that the O–H bond breakage is not the rate-determining over re-Mg_6Al_1-LDH-Pt, and thus the breakage of α-C–H bond is proposed as the key step for GLY oxidation.

As reported previously [45,46], basic group of support commonly serves as active site for hydroxyl activation in alcohol oxidation reactions which may determine the reaction rate. Since the hydroxyl activation as the rate-determining step has been excluded in this work, we further studied the breakage of α-C–H bond promoted by $Pt^{\delta+}$ species. Fig. 6a displays a positive correlation between TOF and $Pt^{\delta+}/(Pt^0 + Pt^{\delta+})$ ratio, indicating the positively charged $Pt^{\delta+}$ serves as the active site toward glycerol

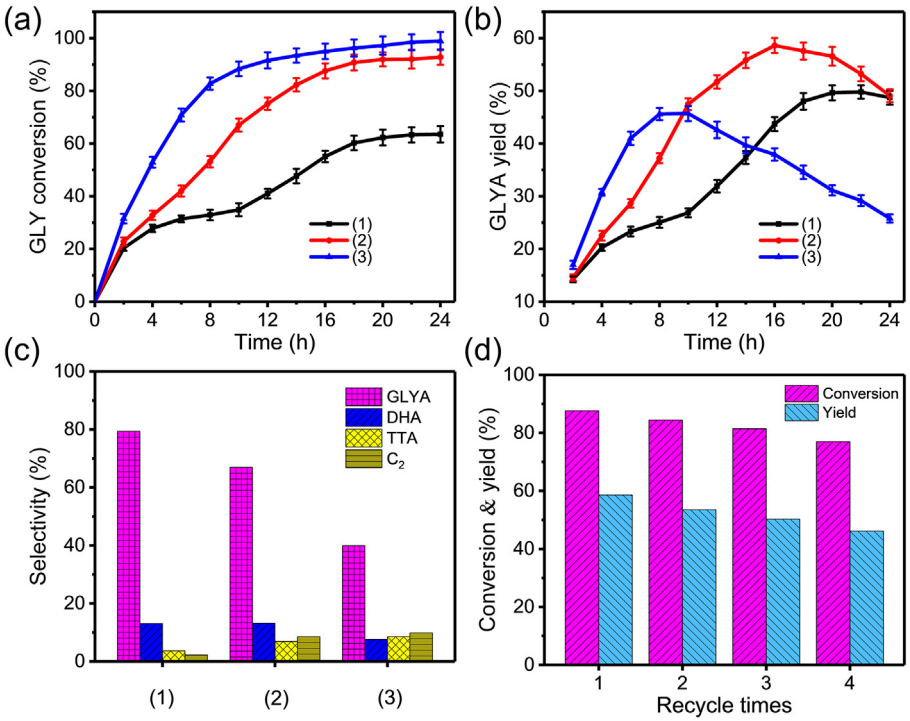

Fig. 4. (Color online) GLY oxidation activity of re-Mg_6Al_1-LDH-Pt. (a) GLY conversion vs. reaction time and (b) GLYA yield vs. reaction time over re-Mg_6Al_1-LDH-Pt with different catalyst dosage. (c) Selectivity toward each product of GLY oxidation at 16 h. (1) GLY/Pt = 1000 (mol:mol), (2) GLY/Pt = 500 (mol:mol), and (3) GLY/Pt = 250 (mol:mol). (d) Catalytic performances over re-Mg_6Al_1-LDH-Pt in 4 consecutive recycles. Reaction conditions: GLY/Pt = 500 (mol:mol); temperature 30 °C; ambient pressure.

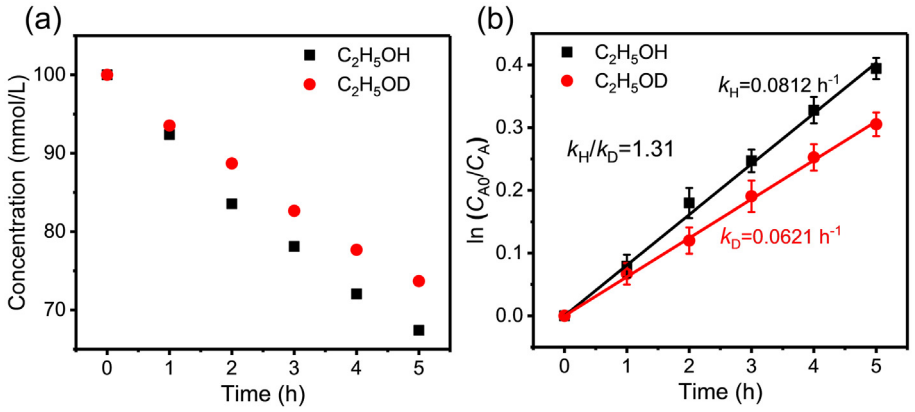

Fig. 5. (Color online) Kinetic isotope experiment of alcohol oxidation over re-Mg_6Al_1-LDH-Pt. (a) Reactant concentration as a function of reaction time and (b) kinetic isotope effect in oxidation of C_2H_5OH and C_2H_5OD. Reaction conditions: H_2O (20 mL), ethanol (2 mmol), catalyst (40 mg), 30 °C, ambient pressure.

oxidation. It has been reported that for alcohol oxidation, the positively charged $M^{\delta+}$ could absorb α-$H^{\delta-}$ more preferably to promote α-C–H breakage [47], leading to an enhanced overall activity. As proved by XANES, FTIR and H_2-TPR, $Pt^{\delta+}$ species were induced from metal-support interaction, which functions as the active site and the relative amount of $Pt^{\delta+}$ were regulated successfully by Mg/Al ratio. Furthermore, metallic Pt^0 is still indispensable in glycerol aerobic oxidation, owing to its capability for the activation absorption and dissociation of oxygen.

Although the basicity of support is regarded as insignificant in this reaction, it affects the product selectivity due to the difference in product acidity. To investigate this issue, we correlate DHA selectivity and GLYA selectivity with surface basicity, respectively. As shown in Fig. 6b, the curve of DHA selectivity vs. surface basicity exhibits a monotonic decrease from re-Mg_2Al_1-LDH-Pt to re-Mg_8Al_1-LDH-Pt, indicating that basic site is more inclined to promote oxidation of terminal-hydroxyl rather than central-hydroxyl. Nevertheless, as the parallel product, GLYA does not show an opposite trend against DHA but displays increase firstly and then decrease at Mg/Al = 8 (Fig. 6c). As an organic acid product, GLYA is prone to adsorb on the basic sites of support once generated, which may result in its over-oxidation and thus declined selectivity. One conclusion can be drawn that a medium basicity of support (e.g., re-Mg_6Al_1-LDH) promotes the oxidation of terminal-hydroxyl and the desorption of target product GLYA, accounting for the largest selectivity.

Some previous reports claimed that glycerol undergoes oxidation to generate DHA at first and then DHA is oxidized to form GLYA and other C_2-products [6]. To prove this issue, the oxidation of DHA over re-Mg_6Al_1-LDH-Pt was investigated under the same conditions as for GLY oxidation reaction (Fig. S5 online). The results show that DHA conversion reaches 10.3% at 2 h and remains constant. This indicates that DHA cannot be produced in majority in this catalytic system and GLYD is the initial product (Fig. S7 online). Based on the structural characterizations and catalytic evaluations in this work, coupled with previous studies [48], a possible catalytic mechanism is proposed in Scheme 1. Initially, terminal-hydroxyl of glycerol is absorbed by basic site to give α-$C^{\delta+}$–$H^{\delta-}$ structure while O_2 molecule undergoes dissociation adsorption to produce active O species on metallic Pt^0 site. Subsequently, proton-H in terminal-hydroxyl reacts with surficial basic hydroxyl on support to release one molecule of water, accompanied by the formation of alkoxide species. In the third step, bond cleavage of α-$C^{\delta+}$–$H^{\delta-}$ occurs to form GLYD and $Pt^{\delta+}$–$H^{\delta-}$ species which reacts with active O species to produce hydroxyl on Pt^0 site. Most importantly, the fracture of α-$C^{\delta+}$–$H^{\delta-}$ bond (rate-determining step) is accelerated by the positively charged $Pt^{\delta+}$ site, which enhances the activity of glycerol oxidation.

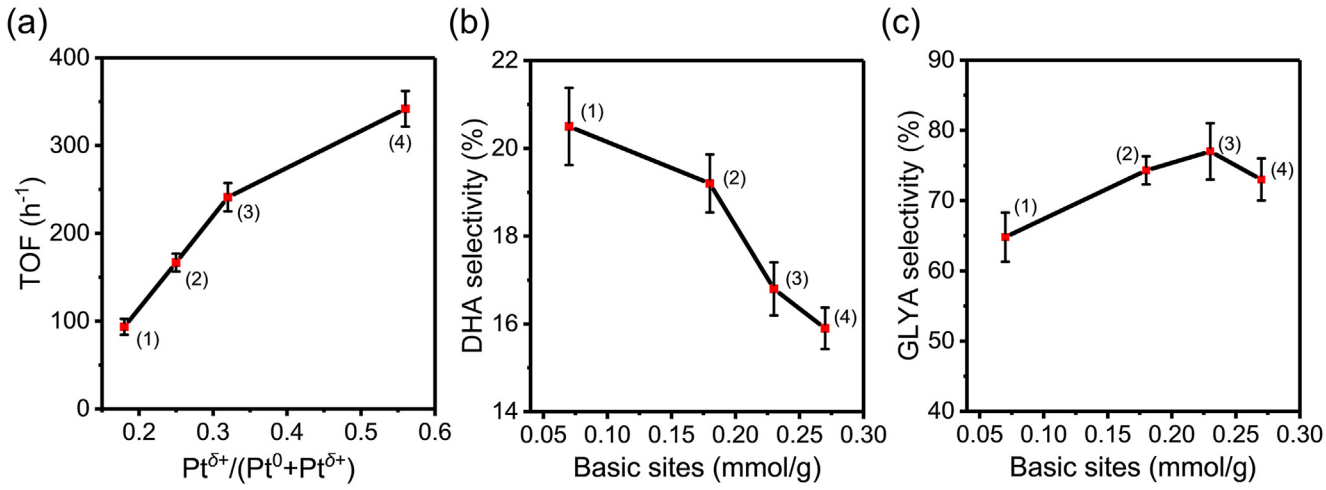

Fig. 6. (Color online) Correlations between the activity and the structure of re-Mg_xAl_1-LDH-Pt samples. Profiles of (a) TOF value vs. $Pt^{\delta+}/(Pt^{\delta+} + Pt^0)$ ratio; (b) DHA selectivity vs. support basicity and (c) GLYA selectivity vs. support basicity. (1) re-Mg_2Al_1-LDH-Pt, (2) re-Mg_4Al_1-LDH-Pt, (3) re-Mg_6Al_1-LDH-Pt, and (4) re-Mg_8Al_1-LDH-Pt.

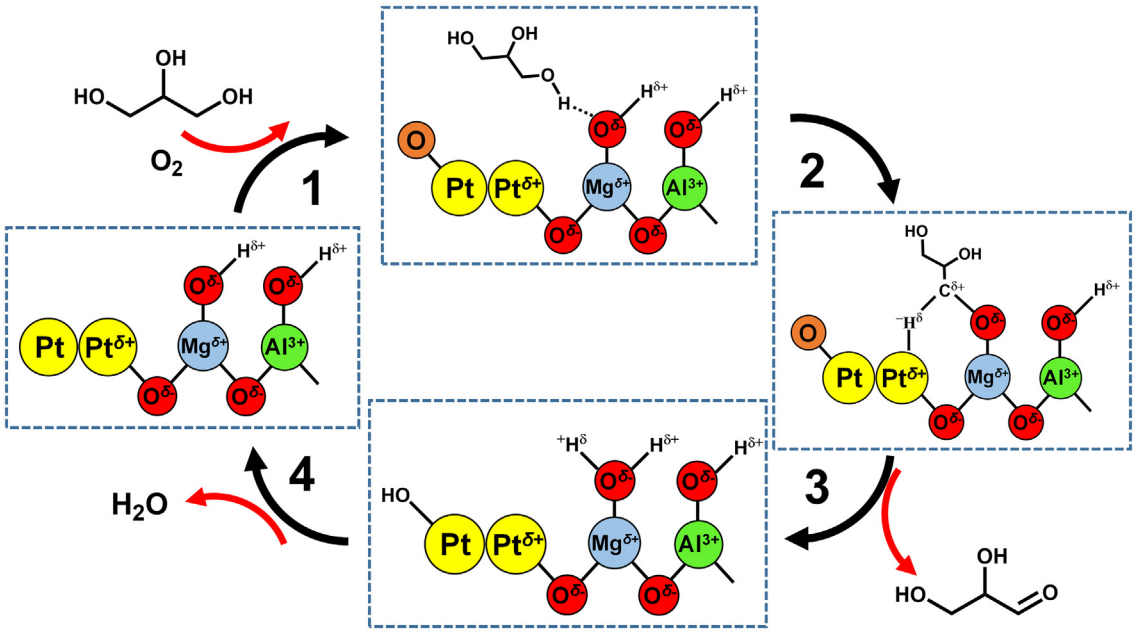

Scheme 1. (Color online) Schematic reaction pathway for the first step of glycerol oxidation: from glycerol to glyceraldehyde over re-Mg_xAl_1-LDH-Pt catalyst.

5. Conclusion

In this work, Pt nanoparticles supported on rehydrated Mg_xAl_1-LDH were prepared by a facile impregnation-reduction method followed by an *in situ* rehydration process. The target catalyst re-Mg_6Al_1-LDH exhibits an excellent catalytic performance for the selective glycerol oxidation to glyceric acid (TOF: 241.1 h^{-1}; GLY conversion: 87.6%; GLYA yield: 58.6%), which attains a high level compared with previous reports. A combination study including *quasi in situ* XANS, *in situ* CO-FTIR, and H_2-TPR confirms that interfacial $Pt^{\delta+}$ species are generated through metal-support interaction, which serve as active site by accelerating the rate-determining step (α-C–H bond fracture). Moreover, the correlation between product selectivity and support basicity reveals that basic sites of catalyst favor the oxidation of terminal-hydroxyl to produce GLYA. However, a high basicity would diminish GLYA yield due to its over-oxidation. This work provides a facial strategy to greatly improve catalytic performance of glycerol oxidation although few insufficiencies such as catalyst stability still remain to be solved.

Conflict of interest

The authors declare that they have no conflict of interest.

Acknowledgments

This work was supported by the National Natural Science Foundation of China (21871021 and 21521005), the National Key Research and Development Program (2017YFA0206804), and the Fundamental Research Funds for the Central Universities (buctylkxj01 and XK1802-6).

Author contributions

Min Wei and Shuxian Shi conceived the idea, supervised the project, and analyzed data. Junbo Zhang conducted experiments and analyzed the data. Xiaolin Li, Ming Xu, Yusen Yang, Yinwen Li, Ning Liu, Xiaoyu Meng and Lifang Chen assisted the structural characterizations and catalytic experiments. Junbo Zhang and Yusen Yang co-wrote the manuscript. All the authors discussed the results and contributed to the preparation of the manuscript.

Appendix A. Supplementary materials

Supplementary materials to this article can be found online at https://doi.org/10.1016/j.scib.2019.10.003.

References

[1] Lee AF, Bennett JA, Manayil JC, et al. Heterogeneous catalysis for sustainable biodiesel production via esterification and transesterification. Chem Soc Rev 2014;43:7887–916.
[2] Li D, Xin H, Du X, et al. Recent advances for the production of hydrocarbon biofuel via deoxygenation progress. Sci Bull 2015;60:2096–106.
[3] Dodekatos G, Schünemann S, Tüysüz H. Recent advances in thermo-, photo-, and electrocatalytic glycerol oxidation. ACS Catal 2018;8:6301–33.
[4] León-Reina L, Cabeza A, Rius J, et al. Structural and surface study of calcium glyceroxide, an active phase for biodiesel production under heterogeneous catalysis. J Catal 2013;300:30–6.
[5] Schünemann S, Schüth F, Tüysüz H. Selective glycerol oxidation over ordered mesoporous copper aluminum oxide catalysts. Catal Sci Technol 2017;7:5614–24.
[6] Liu S-S, Sun K-Q, Xu B-Q. Specific selectivity of Au-catalyzed oxidation of glycerol and other C3-polyols in water without the presence of a base. ACS Catal 2014;4:2226–30.
[7] Zheng L, Li X, Du W, et al. Metal-organic framework derived Cu/ZnO catalysts for continuous hydrogenolysis of glycerol. Appl Catal B 2017;203:146–53.
[8] An S, Sun Y, Song D, et al. Arenesulfonic acid-functionalized alkyl-bridged organosilica hollow nanospheres for selective esterification of glycerol with lauric acid to glycerol mono- and dilaurate. J Catal 2016;342:40–54.
[9] Morales-Marín A, Ayastuy JL, Iriarte-Velasco U, et al. Nickel aluminate spinel-derived catalysts for the aqueous phase reforming of glycerol: effect of reduction temperature. Appl Catal B 2019;244:931–45.
[10] Zhu S, Gao X, Zhu Y, et al. SiO_2 promoted $Pt/WO_x/ZrO_2$ catalysts for the selective hydrogenolysis of glycerol to 1,3-propanediol. Appl Catal B 2014;158–159:391–9.
[11] Castanheiro JE, Vital J, Fonseca IM, et al. Glycerol conversion into biofuel additives by acetalization with pentanal over heteropolyacids immobilized on zeolites. Catal Today 2019. https://doi.org/10.1016/j.cattod.2019.04.048.
[12] Li Y, Zaera F. Sensitivity of the glycerol oxidation reaction to the size and shape of the platinum nanoparticles in Pt/SiO_2 catalysts. J Catal 2015;326:116–26.
[13] Ning X, Li Y, Yu H, et al. Promoting role of bismuth and antimony on Pt catalysts for the selective oxidation of glycerol to dihydroxyacetone. J Catal 2016;335:95–104.

[14] Wang W, Jing W, Sheng L, et al. Pd_3Cu coupling with nitrogen-doped mesoporous carbon to boost performance in glycerol oxidation. Appl Catal A 2017;538:123–30.
[15] Liang D, Gao J, Wang J, et al. Selective oxidation of glycerol in a base-free aqueous solution over different sized Pt catalysts. Catal Commun 2009;10:1586–90.
[16] Tongsakul D, Nishimura S, Ebitani K. Platinum/gold alloy nanoparticles-supported hydrotalcite catalyst for selective aerobic oxidation of polyols in base-free aqueous solution at room temperature. ACS Catal 2013;3:2199–207.
[17] Xu J, Zhang H, Zhao Y, et al. Selective oxidation of glycerol to lactic acid under acidic conditions using AuPd/TiO_2 catalyst. Green Chem 2013;15:1520–5.
[18] Liang D, Gao J, Sun H, et al. Selective oxidation of glycerol with oxygen in a base-free aqueous solution over MWNTs supported Pt catalysts. Appl Catal B 2011;106:423–32.
[19] Xu C, Du Y, Li C, et al. Insight into effect of acid/base nature of supports on selectivity of glycerol oxidation over supported Au-Pt bimetallic catalysts. Appl Catal B 2015;164:334–43.
[20] Zhang M, Shi J, Ning W, et al. Reduced graphene oxide decorated with PtCo bimetallic nanoparticles: facile fabrication and application for base-free oxidation of glycerol. Catal Today 2017;298:234–40.
[21] Yang L, Li X, Sun Y, et al. Selective oxidation of glycerol in base-free conditions over N-doped carbon film coated carbon supported Pt catalysts. Catal Commun 2017;101:107–10.
[22] Zhang C, Yue H, Huang Z, et al. Hydrogen production via steam reforming of ethanol on phyllosilicate-derived Ni/SiO_2: enhanced metal–support interaction and catalytic stability. ACS Sustainable Chem Eng 2013;1:161–73.
[23] Liu N, Xu M, Yang Y, et al. $Au^{\delta-}$–O_v–Ti^{3+} interfacial site: catalytic active center toward low-temperature water gas shift reaction. ACS Catal 2019;9:2707–17.
[24] Ning X, Yu H, Peng F, et al. Pt nanoparticles interacting with graphitic nitrogen of N-doped carbon nanotubes: effect of electronic properties on activity for aerobic oxidation of glycerol and electro-oxidation of Co. J Catal 2015;325:136–44.
[25] Sun Y, Li X, Wang J, et al. Carbon film encapsulated Pt NPs for selective oxidation of alcohols in acidic aqueous solution. Appl Catal B 2017;218:538–44.
[26] Yan T, Bing W, Xu M, et al. Acid-base sites synergistic catalysis over Mg-Zr-Al mixed metal oxide toward synthesis of diethyl carbonate. RSC Adv 2018;8:4695–702.
[27] Liu J, Xu S, Bing W, et al. Cu-decorated Ru catalysts supported on layered double hydroxides for selective benzene hydrogenation to cyclohexene. ChemCatChem 2015;7:846–55.
[28] Liu J, Zou S, Lu L, et al. Room temperature selective oxidation of benzyl alcohol under base-free aqueous conditions on Pt/TiO_2. Catal Commun 2017;99:6–9.
[29] Liu J, Zou S, Wu J, et al. Green catalytic oxidation of benzyl alcohol over Pt/ZnO in base-free aqueous medium at room temperature. Chin J Catal 2018;39:1081–9.
[30] van Laar FMPR, De Vos DE, Pierard F, et al. Generation of singlet molecular oxygen from H_2O_2 with molybdate-exchanged layered double hydroxides: effects of catalyst composition and reaction conditions. J Catal 2001;197:139–50.
[31] Zhou W, Tao Q, Pan J, et al. Effect of basicity on the catalytic properties of Ni-containing hydrotalcites in the aerobic oxidation of alcohol. J Mol Catal A Chem 2016;425:255–65.
[32] Zvoianu R, Birjega R, Pavel O, et al. Hydrotalcite like compounds with low Mo-loading active catalysts for selective oxidation of cyclohexene with hydrogen peroxide. Appl Catal A 2005;286:211–20.
[33] Liu P, Zhao Y, Qin R, et al. A vicinal effect for promoting catalysis of Pd_1/TiO_2: supports of atomically dispersed catalysts play more roles than simply serving as ligands. Sci Bull 2018;63:675–82.
[34] Zhu Y, An Z, He J. Single-atom and small-cluster Pt induced by Sn (IV) sites confined in an LDH lattice for catalytic reforming. J Catal 2016;341:44–54.
[35] Zhu Y, An Z, Song H, et al. Lattice-confined Sn (IV/II) stabilizing raft-like Pt clusters: high selectivity and durability in propane dehydrogenation. ACS Catal 2017;7:6973–8.
[36] Ren G-Q, Pei G-X, Ren Y-J, et al. Effect of group IB metals on the dehydrogenation of propane to propylene over anti-sintering Pt/$MgAl_2O_4$. J Catal 2018;366:115–26.
[37] Tong T, Liu X, Guo Y, et al. The critical role of CeO_2 crystal-plane in controlling pt chemical states on the hydrogenolysis of furfuryl alcohol to 1,2-pentanediol. J Catal 2018;365:420–8.
[38] Xu M, He S, Chen H, et al. TiO_{2-x}-modified Ni nanocatalyst with tunable metal-support interaction for water-gas shift reaction. ACS Catal 2017;7:7600–9.
[39] Belskaya OB, Stepanova LN, Gulyaeva TI, et al. Zinc influence on the formation and properties of Pt/Mg(Zn)AlO_x catalysts synthesized from layered hydroxides. J Catal 2016;341:13–23.
[40] Liu L, Zhou F, Wang L, et al. Low-temperature CO oxidation over supported Pt, Pd catalysts: particular role of FeO_x support for oxygen supply during reactions. J Catal 2010;274:1–10.
[41] Zhou C-H, Beltramini JN, Lin C-X, et al. Selective oxidation of biorenewable glycerol with molecular oxygen over Cu-containing layered double hydroxide-based catalysts. Catal Sci Technol 2011;1:111–22.
[42] Yuan Z, Gao Z, Xu B-Q. Acid-base property of the supporting material controls the selectivity of Au catalyst for glycerol oxidation in base-free water. Chin J Catal 2015;36:1543–51.
[43] Villa A, Chan-Thaw CE, Prati L. Au NPs on anionic-exchange resin as catalyst for polyols oxidation in batch and fixed bed reactor. Appl Catal B 2010;96:541–7.
[44] Ning X, Zhan L, Wang H, et al. Deactivation and regeneration of *in situ* formed bismuth-promoted platinum catalyst for the selective oxidation of glycerol to dihydroxyacetone. New J Chem 2018;42:18837–43.
[45] Li C, Kawada H, Sun X, et al. Highly efficient alcohol oxidation on nanoporous VSB-5 nickel phosphate catalyst functionalized by NaOH treatment. ChemCatChem 2011;3:684–9.
[46] Shang C, Liu Z-P. Origin and activity of gold nanoparticles as aerobic oxidation catalysts in aqueous solution. J Am Chem Soc 2011;133:9938–47.
[47] Liu W, Sun J, Zhang X, et al. Supported ag catalysts on Mg-Al oxides toward oxidant-free dehydrogenation reaction of benzyl alcohol. Ind Eng Chem Res 2018;57:15606–12.
[48] Du Y, Wang Q, Liang X, et al. Hydrotalcite-like MgMnTi non-precious-metal catalyst for solvent-free selective oxidation of alcohols. J Catal 2015;331:154–61.

Junbo Zhang received his M.S. degree at Beijing University of Chemical Technology in 2019. His research is focused on inorganic heterogeneous catalysis, especially its application in biomass transformation and in production of high value-added chemicals.

Min Wei obtained her B.Eng. degree in 1995 and M.Eng. degree in 1998 from Beijing University of Chemical Technology (BUCT). She subsequently received her Ph.D. from Peking University in 2001, after which she joined the staff of BUCT. She was promoted to full Professor in 2005. She has been a visiting scholar in the Georgia Institute of Technology (in 2008). Her research interests focus on two-dimensional functional materials as well as new catalysts.